Electronic Supplementary Information

Mesogenic Polymer Composites for Temperature-Programmable Thermoelectric Ionogels

Sienoh Park, Byeonggwan Kim,* Cheolhyun Cho, and Eunkyoung Kim*

Department of Chemical and Biomolecular Engineering, Yonsei University, 50 Yonsei-ro, Seodaemun-gu, Seoul 03722, South Korea

E-mail: *Prof. E. Kim, eunkim@yonsei.kr, *Dr. B. Kim, loveichem2@yonsei.ac.kr

Contents

Abbreviation

Abbreviation	Full name
AMPS	2-acrylamido-2-methylpropane sulfonic acid
RM105	4-methoxyphenyl 4-((6-(acryloyloxy)hexyl)oxy)benzoate
PEGDA	poly(ethylene glycol) diacrylate
PEGMEMA	poly(ethylene glycol) methyl ether methacrylate
[EMIM][TFSI]	1-ethyl-3-methylimidazolium bis(trifluoromethylsulfonyl) imide
LCI	liquid crystalline ionogel

Section 1. Materials, methods, and characterization

Materials

2-Acrylamido-2-methylpropane sulfonic acid (AMPS), poly(ethylene glycol) methyl ether methacrylate (average M_n~500), poly(ethylene glycol) diacrylate (average M_n~575), 1-ethyl-3-methylimidazolium bis(trifluoromethylsulfonyl)imide ([EMIM][TFSI]), Rhodamine B, and [4,4'-Bis(1,1-dimethylethyl)-2,2'-bipyridine-N1,N1']bis[2-(2-pyridinyl-N)phenyl-C]iridium(III) hexafluorophosphate ($[Ir(dtbbpy)(ppy)_2]PF_6$) were purchased from Sigma-Aldrich Inc. 2-Hydroxy-4'-(2-hydroxyethoxy)-2-methylpropiophenone (Irgacure 2959) was purchased from Tokyo Chemical Industry Co., Ltd. Deionized water (Extra Pure) was purchased from Duksan General Science. Cerasolzer #186 (indium wire) was purchased from Kuroda Electric Co. LTD. All chemicals were used without further purification.

Characterization

The film morphology images were obtained with a field emission scanning electron microscope (FE-SEM, JSM-6700F, JEOL Korea Ltd.). After fully drying LCI films on ITO glass, Pt sputtering was performed on the sample for 90 s at 10 mA.

Time-of-flight secondary ion mass spectrometer (ToF-SIMS) mapping was performed on the cross-section surface by TOF SIMS 5 (ION TOF GmbH, Münster, Germany) with a 1 keV Cs sputter beam. The diameter of the aperture was set to 100 μm. During the measurement, an 85.2 nA Cs sputter beam with a nominal diameter of 80 nm was rastered over the measurement area. The scan was repeated for 20 min. Mass spectra from 100 × 100 μm^2 areas were taken with Bi_3^+ analyzer beam with a 30 keV in negative polarity using a 0.57 pA beam.

The thickness of the films was measured by an Alpha step profilometer (Tencor Instruments, Alpha-step IQ).

High-resolution X-ray diffraction (HR-XRD) patterns were recorded using a SmartLab, Rigaku, utilizing CuKα radiation (λ=0.154 nm) at a beam power of 9 kW and a step size of 0.02° at a scan speed of 3° min^{-1}. The average polydomain sizes of the three main assigned peaks for LCI12-0, LCI12-2, LCI12-7, LCI8-7, and LCI17-7 were 53.4 nm, 59.8 nm, 74.2 nm, 57.0 nm, and 55.6 nm, respectively, which were determined from the Scherrer equation.[1] 2D grazing-incidence wide-angle X-ray scattering (GIWAXS) patterns were collected at the 3C beam line in the Pohang Accelerator Laboratory (PAL) using a monochromatized 9.8 keV (λ= 0.12651 nm) X-ray irradiation source with a two-dimensional charge-coupled device detector (Rayonix 2D MAR165). The scattering vector (q) was calculated from the equation: $q=4\pi\cdot\sin(\theta)/\lambda$.

UV-vis-NIR spectra (Lambda 750, UV/Vis/NIR Spectrophotometer, PerkinElmer or Avantes) of the LCI films (thickness of 60 and 260 μm) were measured. The FTIR spectra were obtained using a Bruker Tensor 37 FTIR Spectrometer in attenuated total reflectance (ATR) mode with 32 scan and resolution of 1 cm^{-1}. LCI films and compounds were put on ATR window at ~25 °C and 50% RH. At different RH level, the LCI film was put in a humidity controlled chamber for 1 h and FTIR spectrum was quickly measured. For temperature control, the LCI12-7 film was put on the ATR window and heated by using a heatgun while checked the surface temperature using an IR camera. Raman spectroscopy was carried out on a LabRam Aramis spectrometer (Horiba Jovin Yvon) equipped with a 785 nm diode laser, and an 1800 grooves per mm grating that gives a spectral resolution of about 0.21 cm^{-1}. The laser power

was set at 0.5 mW at the sample using a 50× objective. Optical microscopy and polarized light microscopy were performed by using a BA310MET, Motic at ~40% RH.

The LCI films (area of 7 × 7 mm^2) on a 60 μm-thick PET film were placed into a humidity-controlled chamber for 1 h and quickly weighed using a microbalance (Sartorius CPA2P, resolution of 0.001 mg). Thermogravimetric analysis (TGA) was carried out using an SDT Q600 V20.9 Build 20 (TA Instruments) from 25 °C to 600 °C at a heating rate of 10 °C min^{-1} under a N_2 flow of 100 mL min^{-1}.

The tensile tests for LCI films were performed using a universal testing machine (TopTac 2000, Yeonjin Corp. Scientifics Ltd., South Korea). The free-standing LCI films were held by pneumatic grips. The gauge length was adjusted to ~1 cm, and the strain rate was 1 mm s^{-1}. Water contact angle measurements were carried out using a ThetaLite from Dyne Testing Ltd.

The in-plane thermal conductivity (κ) was calculated from the equation $\kappa = C_p\ \alpha\ \rho$, where C_p is the specific heat capacitance, α is the thermal diffusivity, and ρ is the density of the sample. The C_p was measured by differential scanning calorimetry (DSC, 200 F3 Maia, NETZSCH) under N_2 gas flow at a heating rate of 10 °C min^{-1}. The α of the freestanding LCI film (area of 1.2 cm × 1.2 cm) was measured by LFA457, NETZCH in a temperature controllable chamber.

Section 2. Supplementary Tables

Table S1. Composition of the LCI samples.

Sample	Weight, mg							Molar ratio[a]
	AMPS	PEGMEMA	PEGDA	[EMIM][TFSI]	Water	Irgacure 2959	RM105	
LCI8-7	13.0	28.2	3.6	11.0	10.2	0.89	100	1:0.9:0.1:0.45:4
LCI12-7	17.3	18.8	2.4	10.4	13.6	0.87	100	2:0.9:0.1:0.64:6
LCI13-7	19.5	14.1	1.8	10.1	15.3	0.87	100	3:0.9:0.1:0.83:8
LCI15-7	21.7	9.4	1.2	9.9	17.0	0.86	100	5:0.9:0.1:1.20:12
LCI16-7	22.8	7.1	0.9	9.7	17.8	0.85	100	7:0.9:0.1:1.58:16
LCI17-7	23.6	5.1	0.7	9.6	18.5	0.85	100	10:0.9:0.1:2.15:22
LCI12-0	17.3	18.8	2.4	0	13.6	0.87	100	2:0.9:0.1:0:6
LCI12-1	17.3	18.8	2.4	0.52	13.6	0.87	100	2:0.9:0.1:0.03:6
LCI12-2	17.3	18.8	2.4	2.6	13.6	0.87	100	2:0.9:0.1:0.16:6
LCI12-3	17.3	18.8	2.4	3.7	13.6	0.87	100	2:0.9:0.1:0.22:6
LCI12-4	17.3	18.8	2.4	5.2	13.6	0.87	100	2:0.9:0.1:0.32:6
LCI12-5	17.3	18.8	2.4	7.8	13.6	0.87	100	2:0.9:0.1:0.48:6
LCI12-9	17.3	18.8	2.4	13.0	13.6	0.87	100	2:0.9:0.1:0.80:6
LCI12-10	17.3	18.8	2.4	15.7	13.6	0.87	100	2:0.9:0.1:0.96:6

[a] AMPS:PEGMEMA:PEGDA:[EMIM][TFSI]:RM105.

Table S2. Summary of FTIR peak assignment of samples.

Peak, cm^{-1}	AMPS[2, 3]	[EMIM][TFSI][4]	RM105[5, 6]	LCI12-7 (this work)
3437	O-H stretching			
3433				O-H stretching
3240	N-H symmetrical stretching			
3163				aromatic C-H stretching of [EMIM]
3159		aromatic C-H stretching		
3119			aromatic CH stretching	
2993		C-H asymmetrical stretching		
2986	C-H stretching			
2953			aliphatic C-H stretching	
2939				aliphatic C-H stretching
1892-2044			aromatic combination bands	
1728				C=O stretching
1721			C=O stretching	
1666	C=O stretching			
1637			C=C stretching	
1612	C=C stretching			
1606			aromatic ring stretching	aromatic ring stretching
1574		C=N stretching		
1371	S=O asymmetrical stretching			
1352				SO_2 asymmetrical stretching of [TFSI]
1348		SO_2 asymmetrical stretching		
1232	S=O symmetrical stretching			
1074	S=O stretching			
1053		S-N-S asymmetrical stretching		
1039	S=O stretching			
746				CF_3 symmetrical stretching
740		CF_3 symmetrical bending		

The peaks were assigned according to the literature for AMPS,[2, 3] [EMIM][TFSI],[4] and RM105,[5, 6] respectively. LCI12-7 film at 25°C and 50% RH.

Section 3. Supplementary Figures

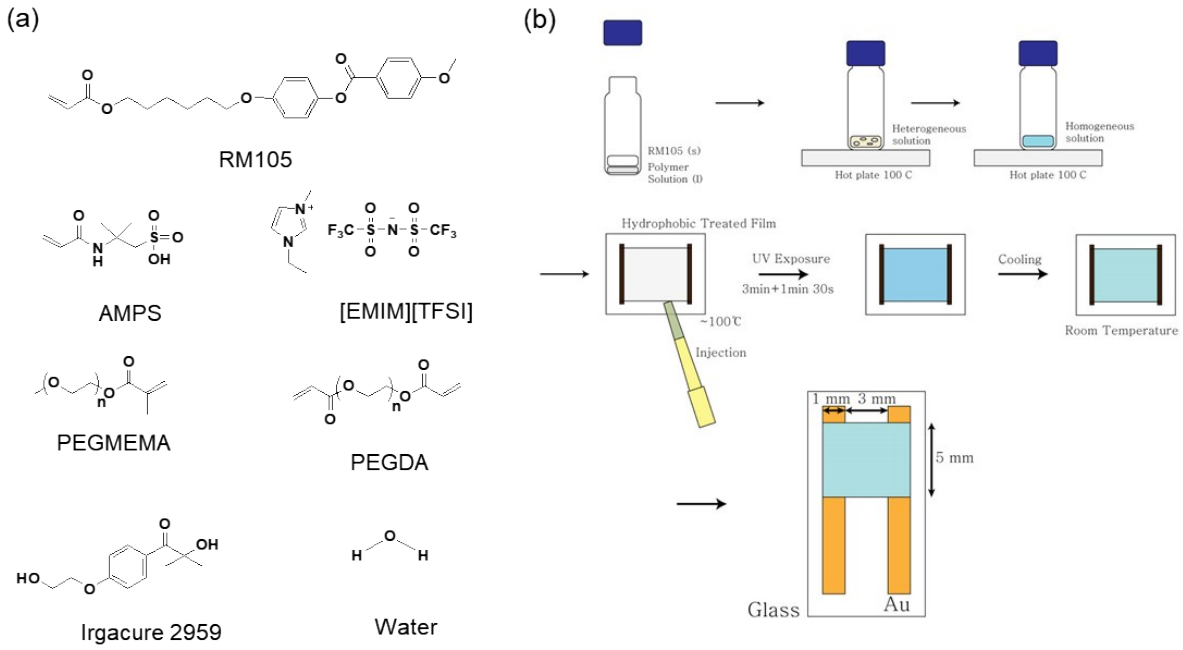

Fig. S1 | Sample preparation. (a) The chemical structures used molecules in this work. (b) Schematic illustration of the LCI film and LCI iTE device preparation.

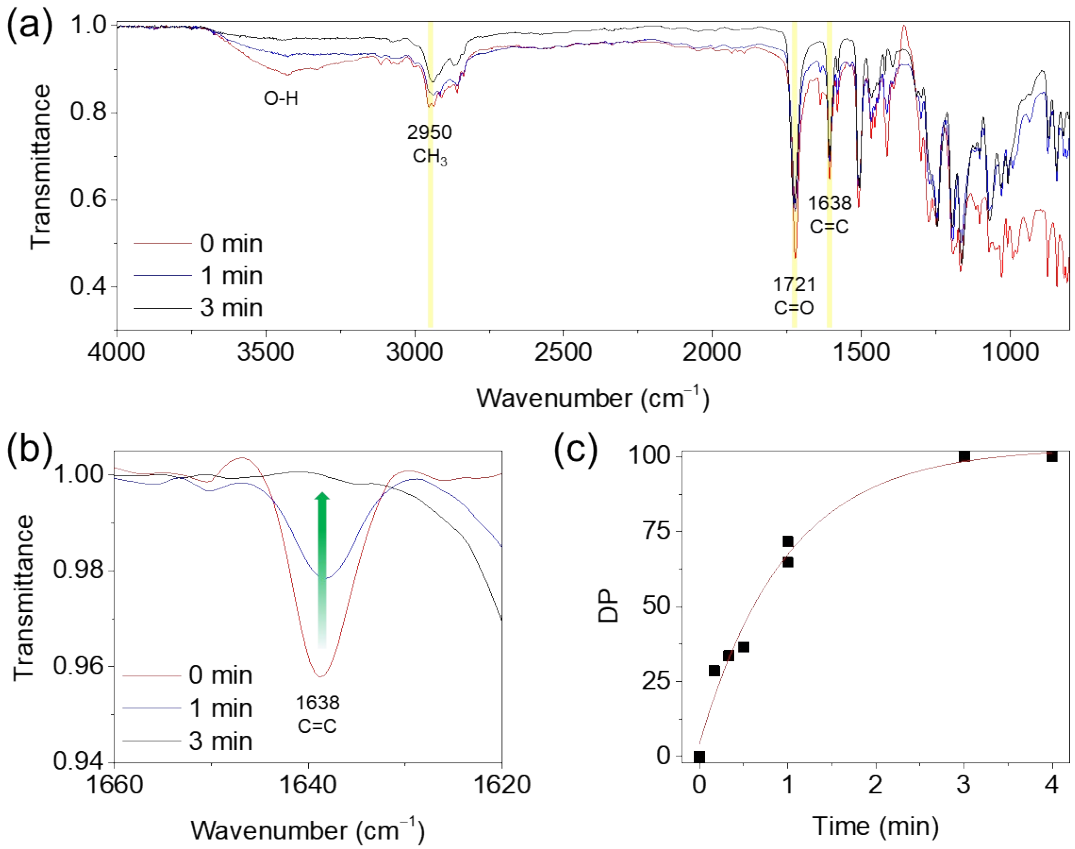

Fig. S2 | FTIR spectroscopy. (a) Ex situ FTIR spectrum for the mixture solution during photopolymerization at different exposure times. (b) The change in the C=C stretching peak at 1638 cm^{-1} over time. (c) Degree of polymerization (DP) of the photoactive monomers in the mixture solution. The normalized peak intensity ratio ($1-\Delta I_{1638}/\Delta I_{1721}$) was used to determine the DP value.

The degree of photopolymerization was monitored by FTIR measurement with increasing exposure time to UV light (Fig. S2)[7, 8]. The peak intensity for the C=C peak of acrylate at 1638 cm^{-1} is decreased compared to the C=O peak of the carbonyl group at 1721 cm^{-1} (internal reference) over time, suggesting photopolymerization of acrylic monomers. The normalized

peak intensity ratio ($1-\Delta I_{1638}/\Delta I_{1721}$) for the C=C peak of acrylate at 1638 cm^{-1} (ΔI_{1638}) in reference to the C=O peak of the carbonyl group (ΔI_{1721}) reaches ~1.0 within 3 min of UV exposure. Therefore, 3 min of UV exposure was set for the photopolymerization of the LCI samples.

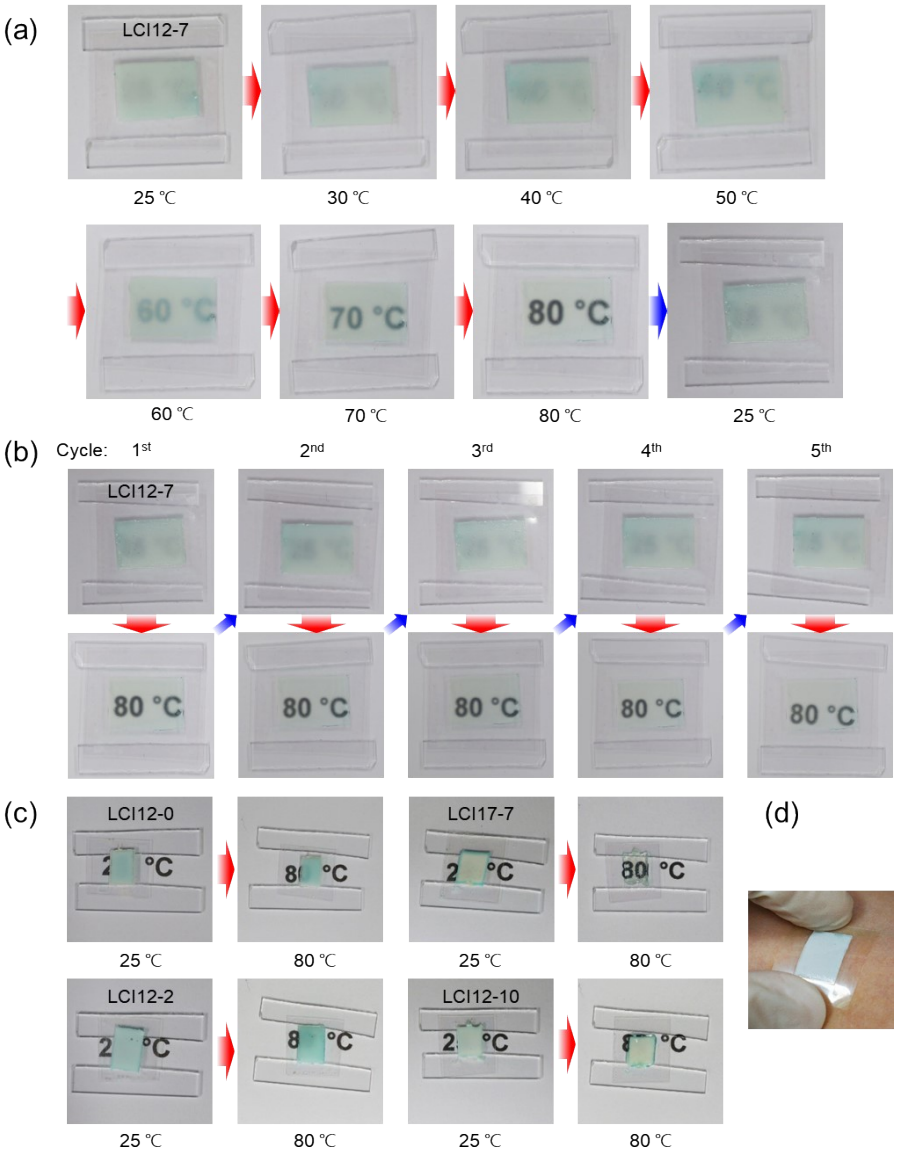

Fig. S3 | Photograph of the films. (a) Photographs of the LCI12-7 film at different system temperatures. (b) Photographs of the LCI12-7 film at 25 °C and 80 °C for 5 heating–cooling cycles. (c) Photographs of the LCI12-0, LCI12-2, LCI12-10, and LCI17-7 films at 25 °C and 80 °C. (d) Photograph of the flexible LCI12-7 film on human skin.

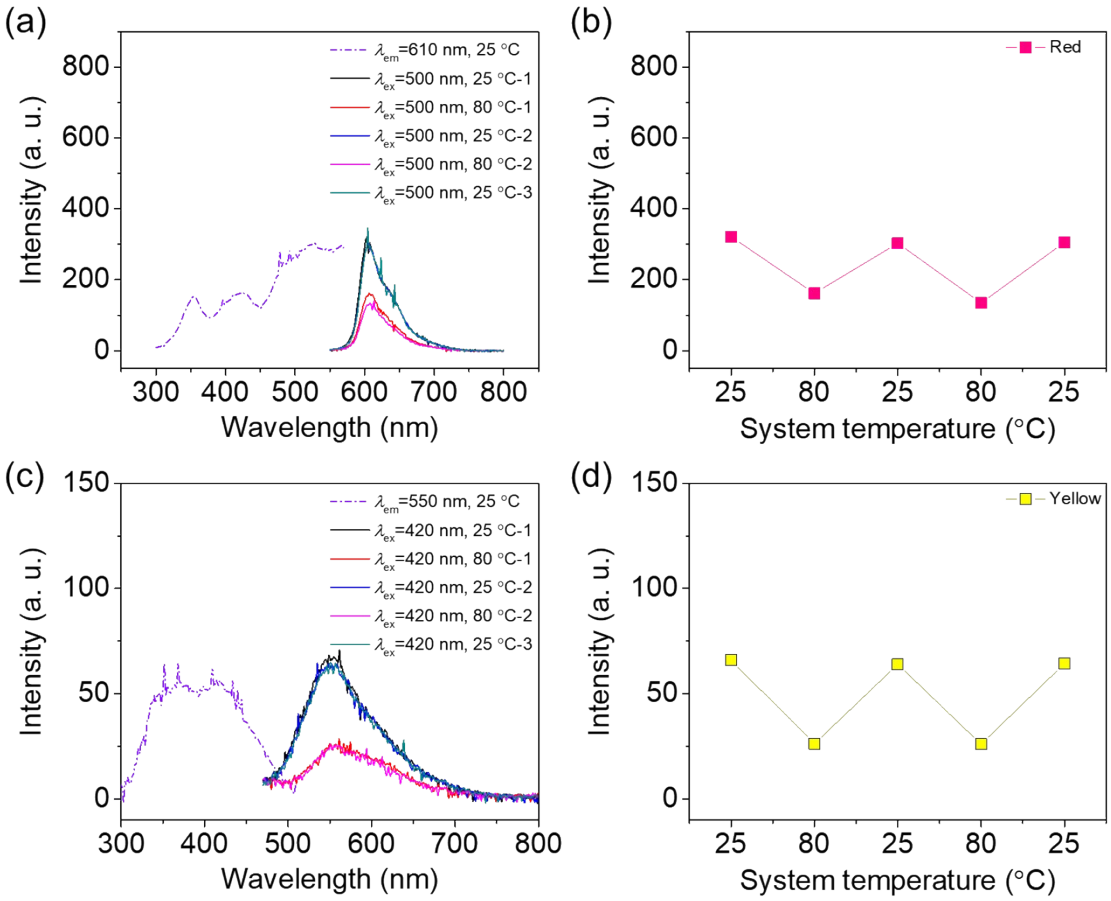

Fig. S4 | Fluorescence spectrum. (a) Excitation (λ_{em} = 610 nm) and emission spectra (λ_{ex} = 490 nm) for the LCI12-7 film containing rhodamine B (0.1 wt%) at different system temperatures of 25 °C and 80 °C for 3 heating–cooling cycles. (b) The corresponding fluorescence intensity at 610 nm. (c) Excitation (λ_{em} = 550 nm) and emission spectra (λ_{ex} = 420 nm) for the LCI12-7 film containing Ir(dtbbpy)(ppy)$_2$PF$_6$ (0.2 wt%) at different system temperatures of 25 °C and 80 °C for 3 heating–cooling cycles. (d) The corresponding fluorescence intensity at 550 nm.

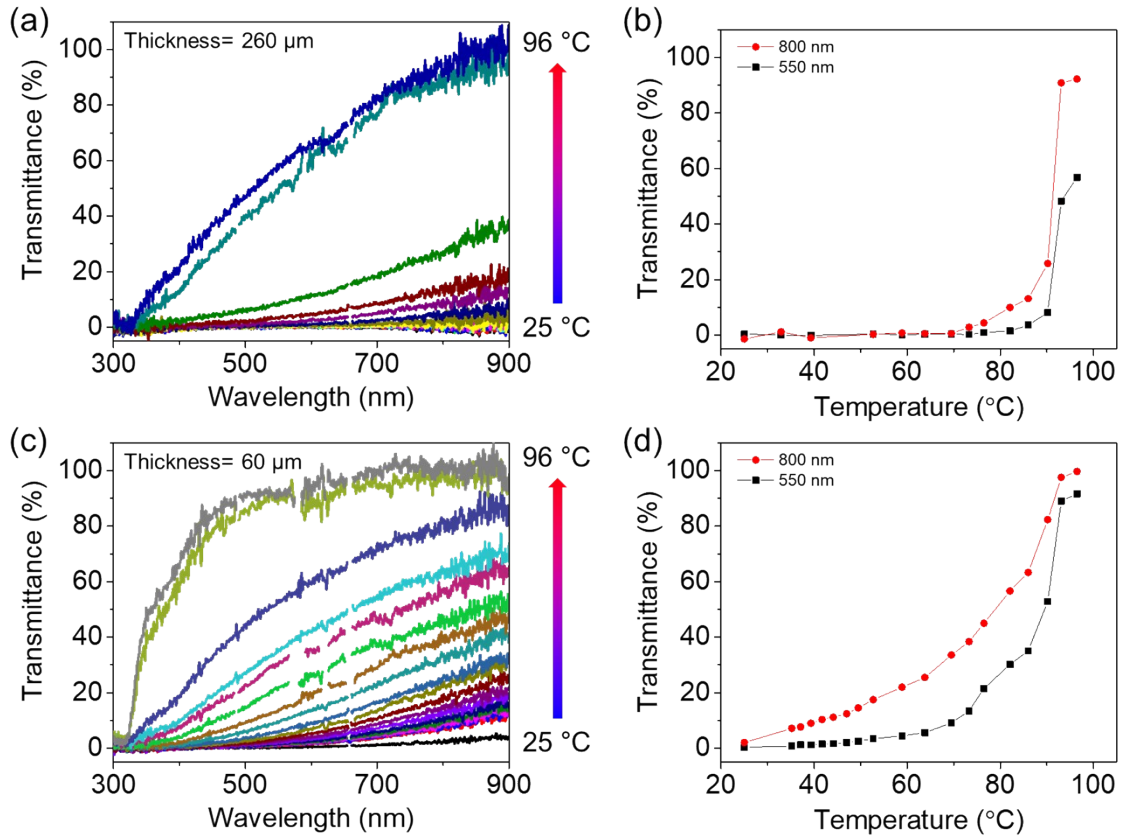

Fig. S5 | Transmittance spectrum. Transmittance of (a) 260 µm thick and (c) 60 µm thick LCI12-7 films at different system temperatures. (b,d) The corresponding transmittance at 550 nm and 800 nm from (a) and (c).

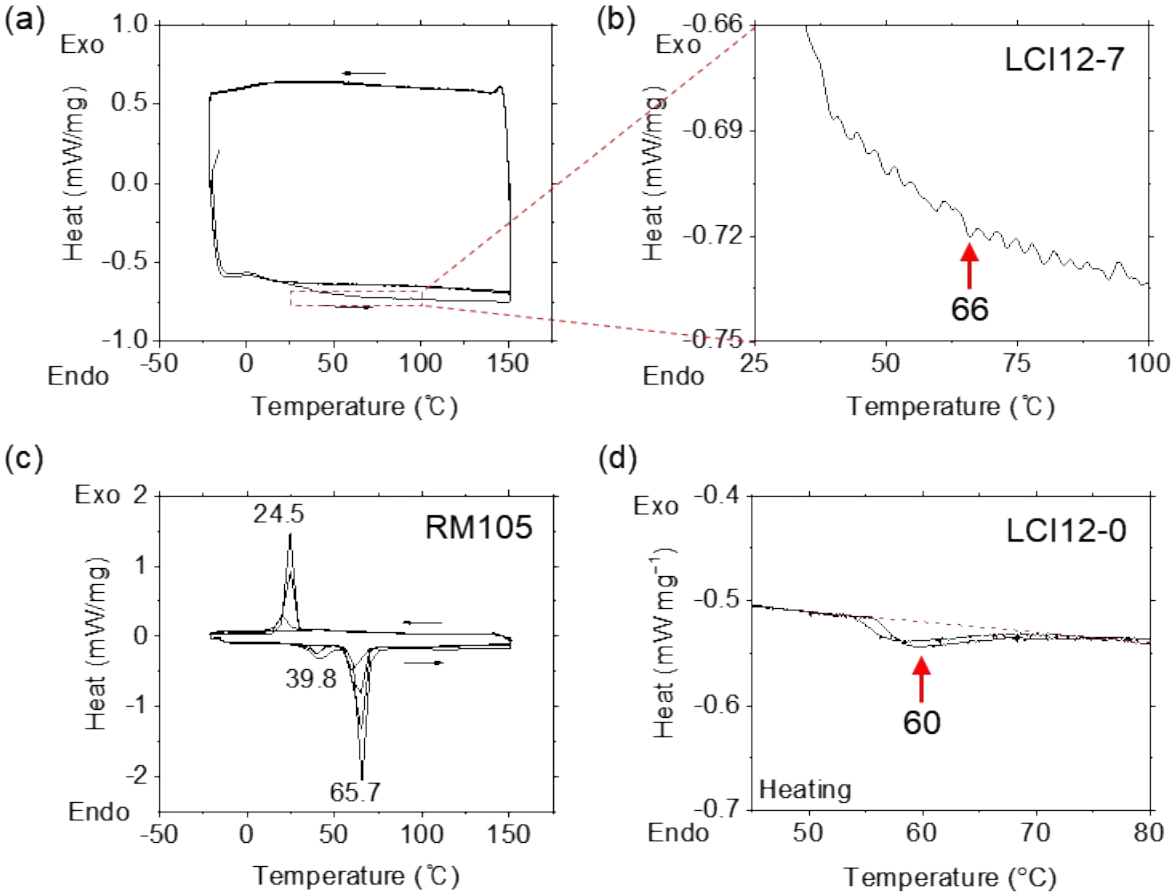

Fig. S6 | Thermal measurement. DSC curves for the (a) LCI12-7 film, (c) RM105, and (d) LCI12-0 film. (b) The enlarged curve from (a).

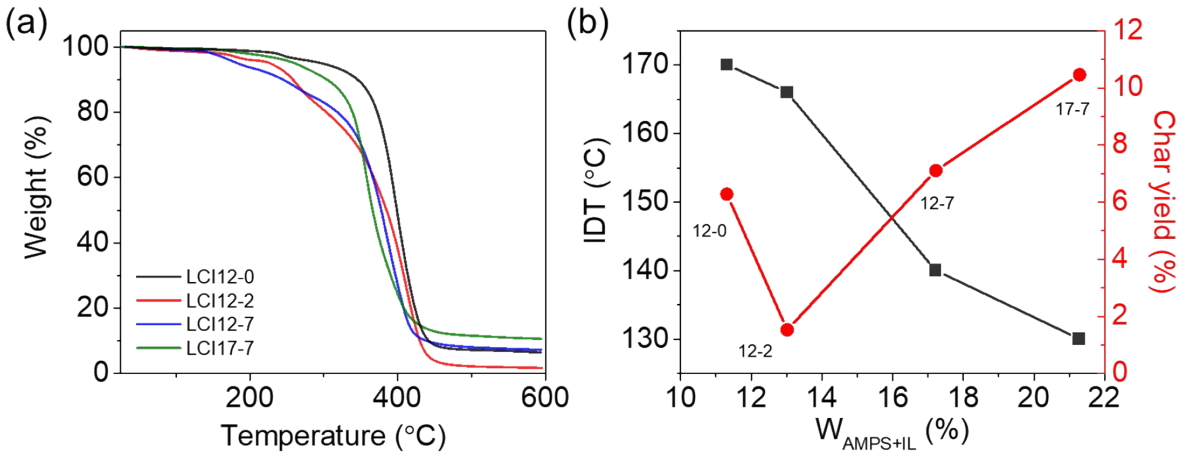

Fig. S7 | Thermal measurement. (a) TGA curves for the LCI films. (b) The corresponding initial decomposition temperature (IDT) and char yield of the LCI films.

Fig. S7a shows the thermogravimetric analysis (TGA) for the LCI films with different AMPS and IL contents. From the TGA curves, the films exhibit a gradual weight loss up to 420 °C. In the temperature range from 60 °C to 130 °C, a small weight loss of less than 2% is observed. This weight loss results from vaporization of absorbed water in the ionogel network and continues with the thermal decomposition of the ionogel. The onset of the decomposition temperature for 5% mass loss for the films without water occurs at 237 °C, 209 °C, and 265 °C for LCI12-2, LCI12-7, and LCI17-7, respectively. The initial decomposition temperature (IDT) is increased to 153 °C for LCI12-2, from 139 °C (LCI12-7) and 130 °C (LCI17-7), indicating that IDT increases as the sum of the AMPS and IL content decreases (Fig. S7b). Thus, the multiple steps of thermal decomposition detected in the TGA curves mainly originate from the decomposition of 1) AMPS due to unstable sulfonic acid that can be degraded to SO_2 or SO_3 (from 200 °C to 388 °C) and 2) cross-linked H-bonds in the ionogel network (degraded from

360 to 420 °C)[9, 10]. The IDT for IL (346 °C)[11] overlaps with the broad decomposition curve of AMPS. RM105, the highest portion (67−71 wt%) in the films, is known to decompose in the temperature range from 360 °C to 400 °C[12]. In addition, char yield significantly increases with the increasing sum of the AMPS and IL content (Fig. S7b).

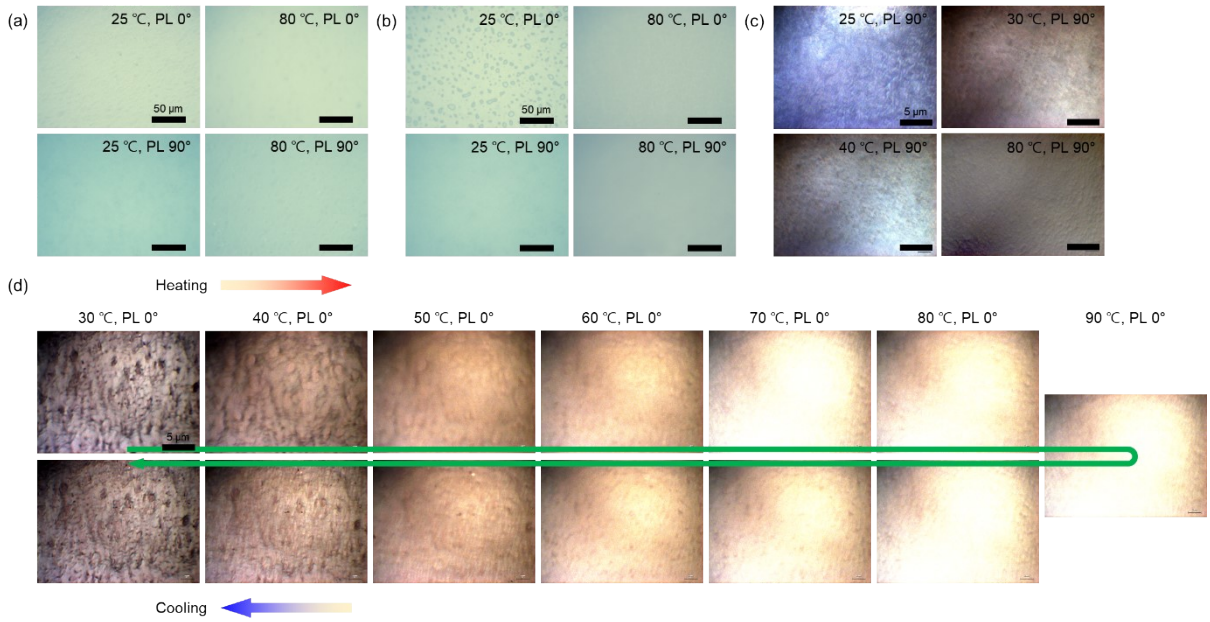

Fig. S8 | POM images. POM images of the (a) LCI12-2 film and (b) LCI17-7 film obtained at 25 °C and 80 °C using 0° and 90° analyzer-polarizers, respectively. (c) POM images of the LCI12-7 films obtained at different temperatures with 90° analyzer-polarizer. (d) POM images of LCI12-7 films obtained at different temperatures with 0° analyzer-polarizer.

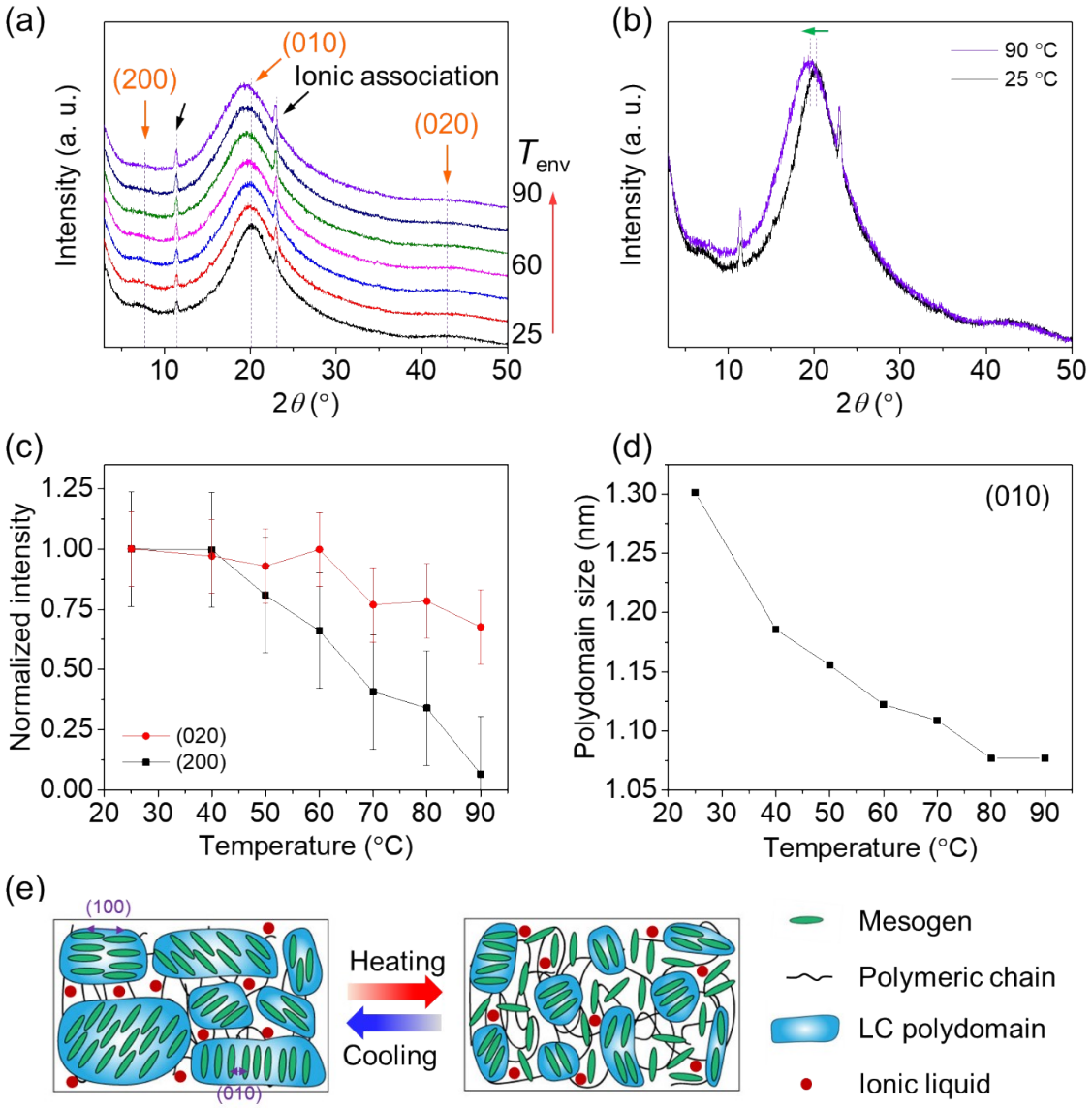

Fig. S9 | HR-XRD patterns with different temperatures. (a) HR-XRD patterns for LCI12-7 film with increasing temperature (T_{env}) from 25 °C to 90 °C. (b) HR-XRD patterns for LCI12-7 film at 25 °C and 90 °C. (c) Normalized peak intensities of (200) and (020) in (a). (d) Polydomain size for the nematic phase (010) determined from the Scherrer equation. (e) Schematic illustration of the nematic-isotropic phase transition in the LCI film with temperature change.

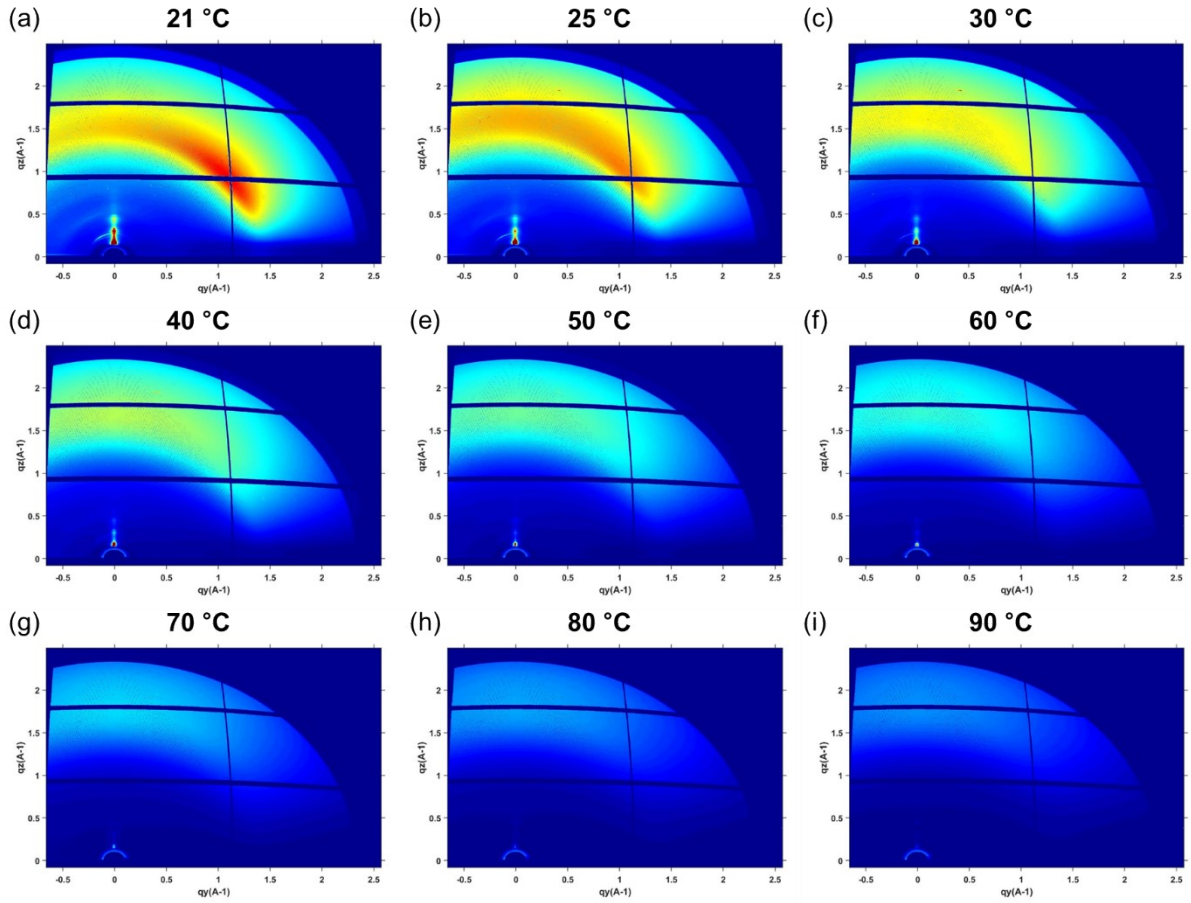

Fig. S10 | 2D GIWAXS patterns of LCI12-7 film with increasing temperature from 21 °C to 90 °C.

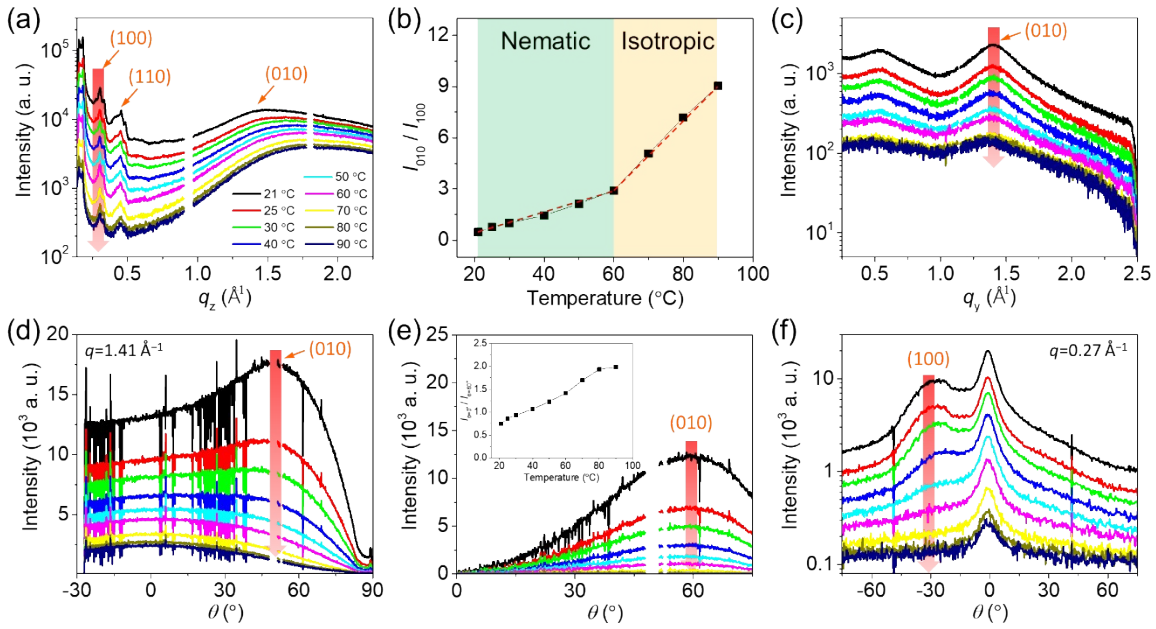

Fig. S11 | q profile of 2D GIWAXS patterns. The (a) out-of-plane (q_z) and (c) in-plane (q_y) profiles of the GIWAXS patterns of the LCI12-7 film. (b) The intensity ratio (I_{010}/I_{100}) of peaks in (a). The azimuthal profile of radial slices at the (d) q=1.41 Å^{-1} and (f) q=1.41 Å^{-1}. θ is the azimuth angle. (e) The azimuthal profile of radial slices at the q=1.41 Å^{-1} after subtracting the scattering background proportional to the azimuthal profile at 90 °C. Inset shows the intensity ratio ($I_{\theta=0^\circ}/I_{\theta=60^\circ}$) of peaks in (d).

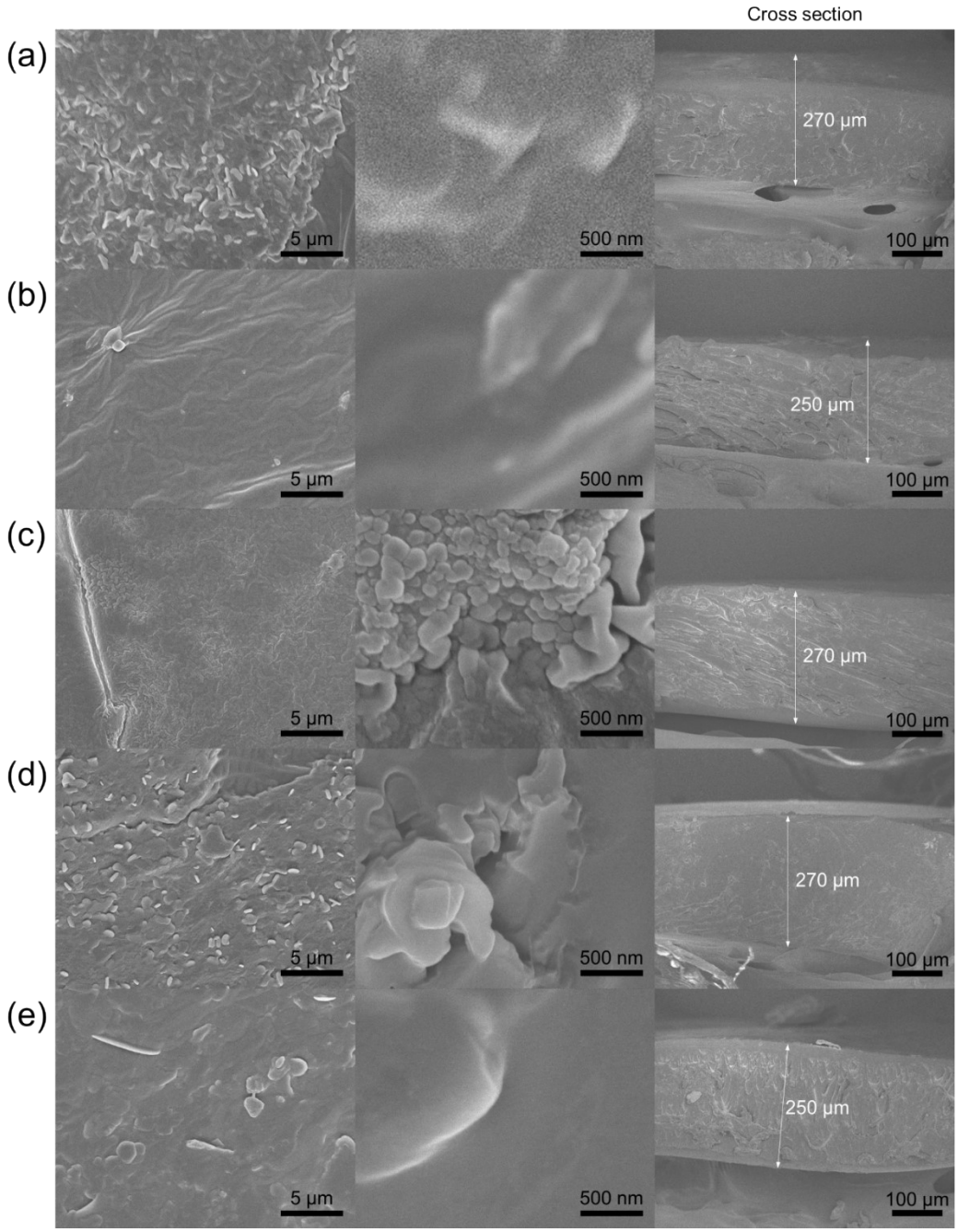

Fig. S12 | Film morphology. SEM images of (a) LCI12-2, (b) LCI12-4, (c) LCI12-7, (d) LCI8-7, and (e) LCI17-7 films. The right column in the images shows the cross-sectional morphology.

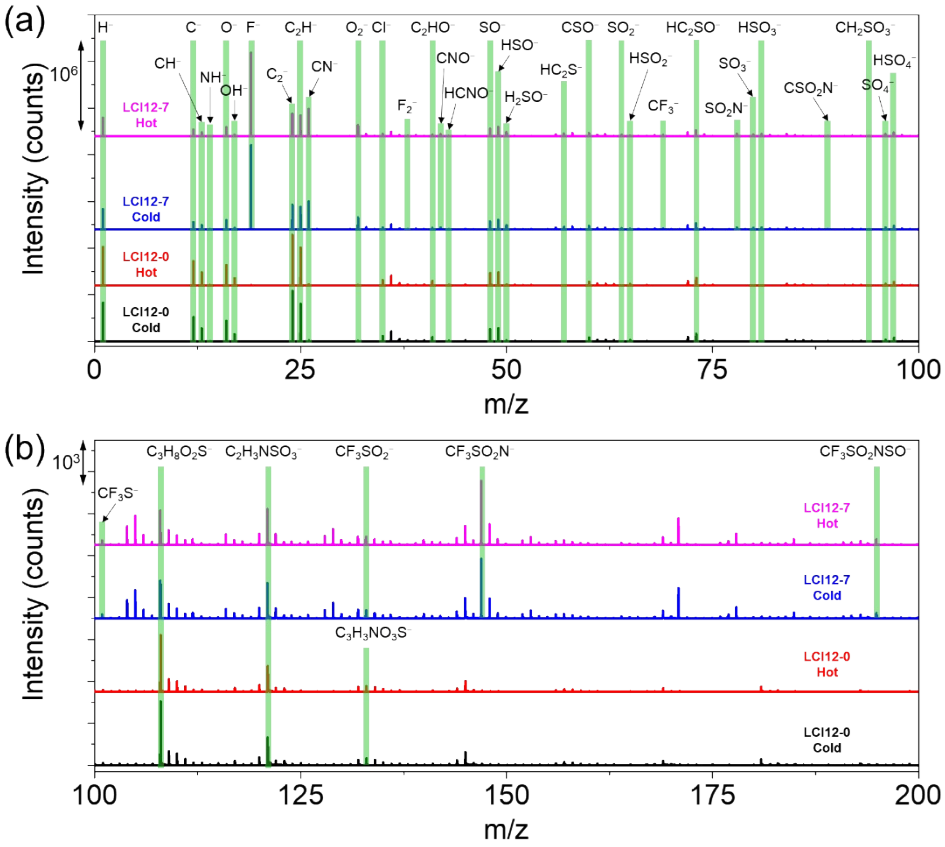

Fig. S13 | ToF-SIMS spectra for LCI12-7 and LCI12-0 films prepared by applying ΔT=8.2 K at 80 °C and 80% RH followed by drying. The mass-to-charge ratios (m/z) ranging (a) from 1 to 100 and (b) from 100 to 200.

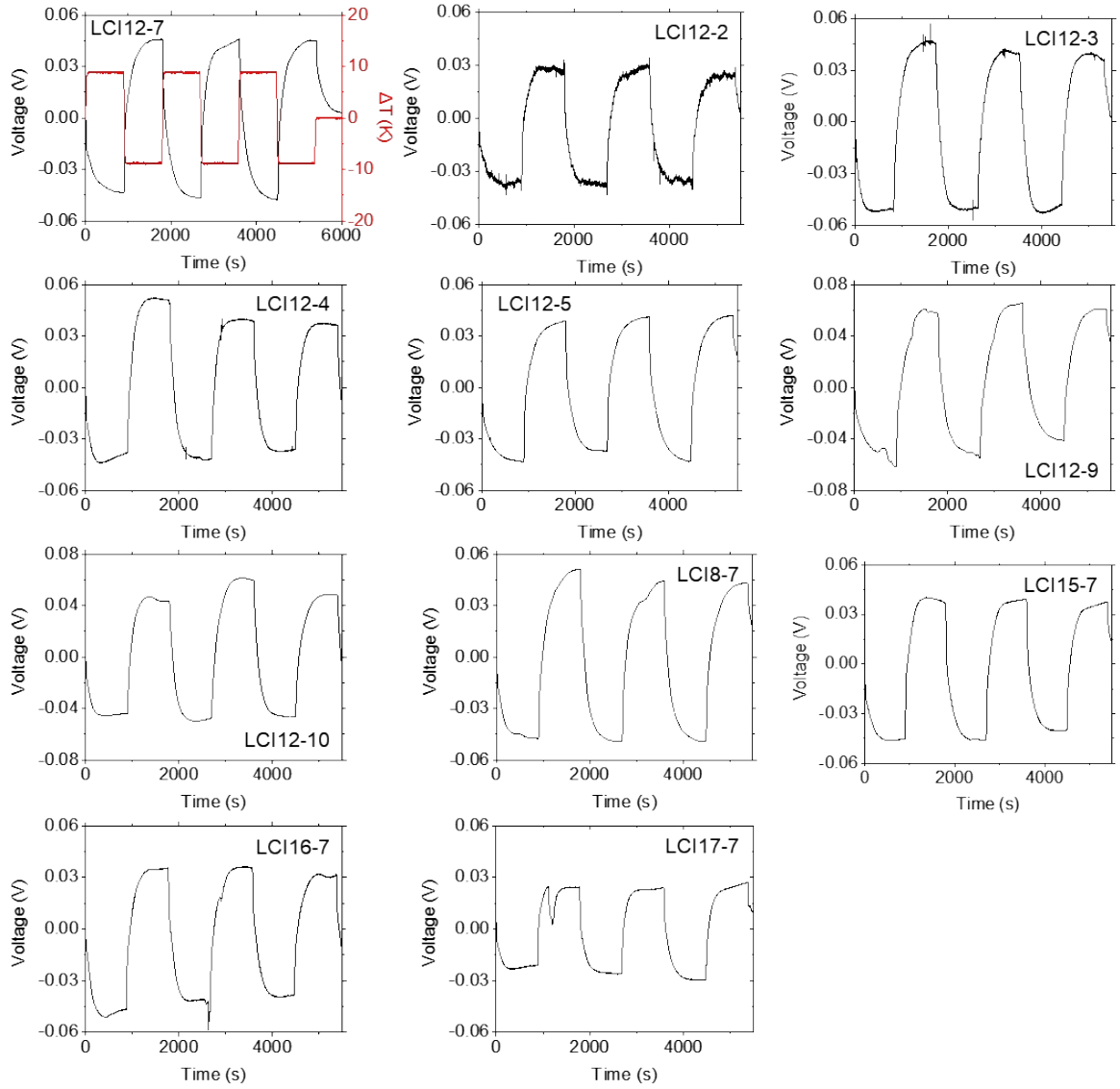

Fig. S14 | Measurement of the ionic Seebeck voltage for LCI films by applying a ΔT=8.2 K at 80 °C and 80% RH.

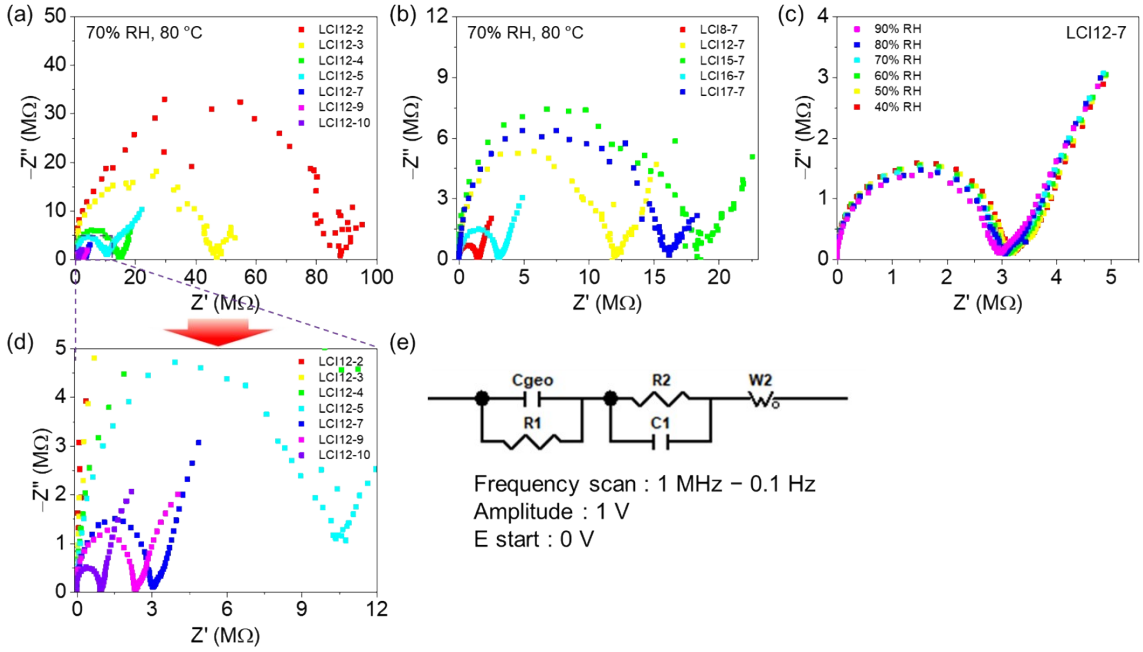

Fig. S15 | EIS analysis. (a,b) LCI films with different compositions at 70% RH and 80 °C. (c) LCI12-7 film at 80 °C with different RH levels. (d) Magnified to the small impedance range of (a). (e) The equivalent circuit model for obtaining each element. R_i was determined from a fit to the electrical circuit.

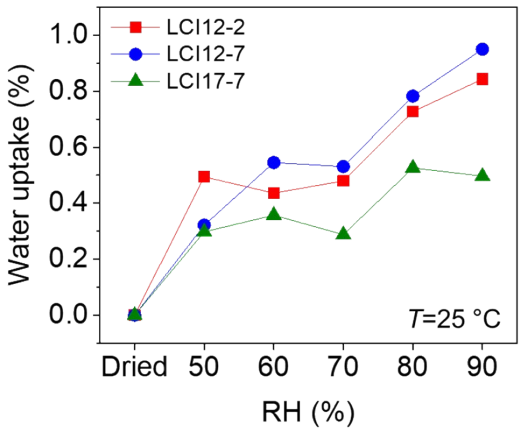

Fig. S16 | Water uptake of the LCI films.

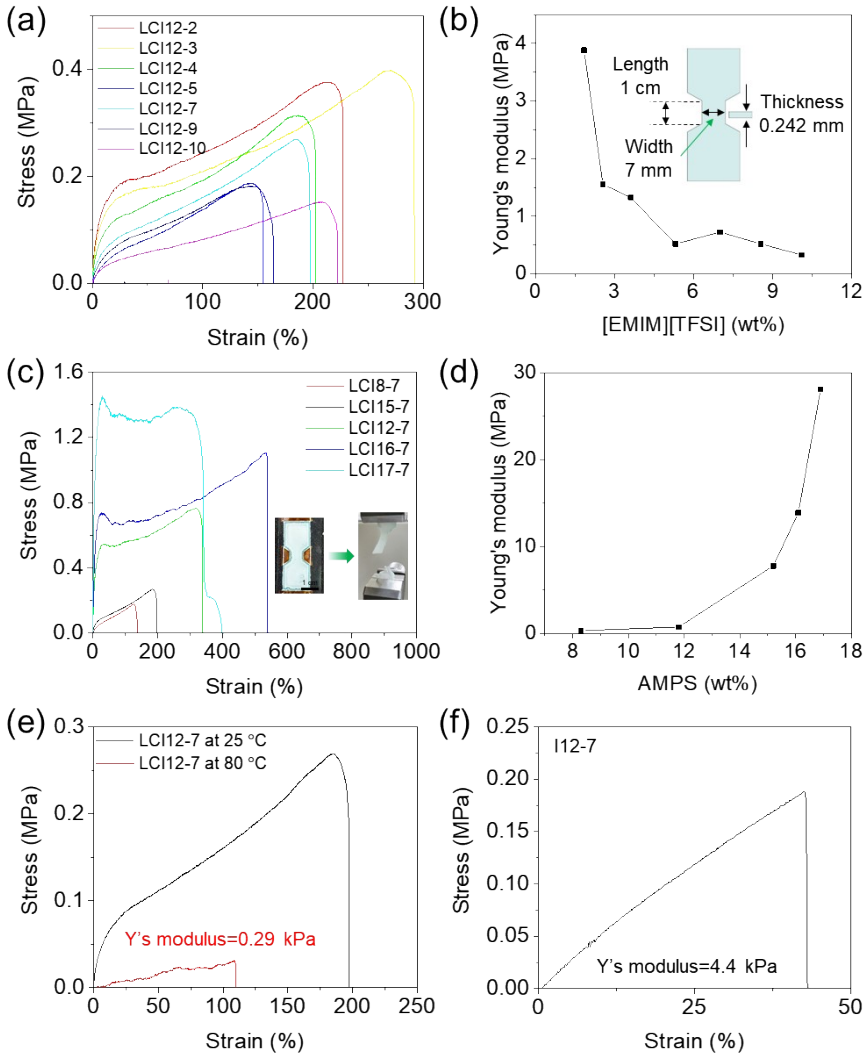

Fig. S17 | Measurement of the mechanical properties of the LCI films. (a) Stress-strain graph for varying [EMIM][TFSI] content. (b) Young's modulus value determined from (a). The inset shows a dog bone-shaped sample with three dimensions. Young's modulus was calculated from the slope of the initial condition. (c) Stress-strain graph for varying AMPS content. Inset photographs show the prepared dog bone-shaped LCI12-7 film and the film after breakage. (d) Young's modulus value determined from (c). Stress-strain graphs obtained for LCI12-7 films at different system temperatures of 25 °C and 80 °C. (g) Stress-strain graph of the I12-7 film.

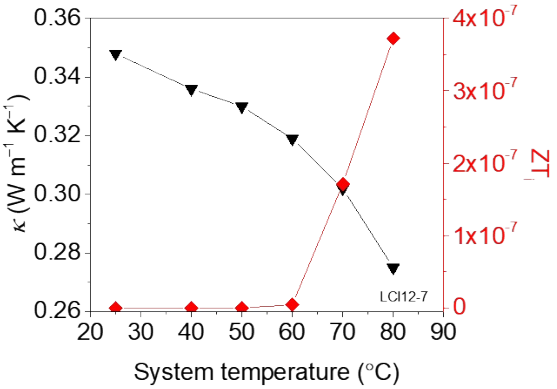

Fig. S18 | Thermal conductivity (κ) and ZT_i value for the LCI12-7 device at different T_{env} values and 80% RH.

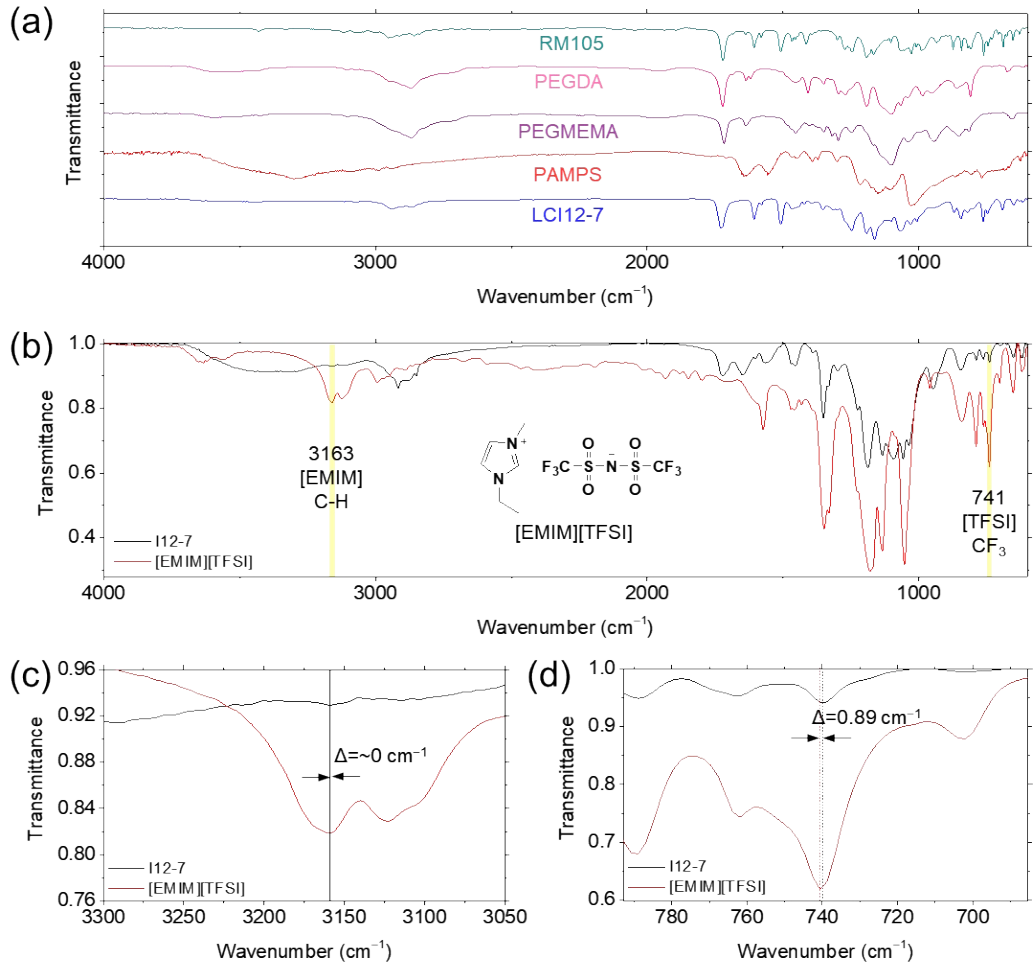

Fig. S19 | FTIR spectroscopy. (a) FTIR spectrum for the components in the LCI films. (b) The assigned peaks for I12-7 and [EMIM][TFSI] for ion transport in the iTE mechanism. (c) The peak shift at 3163 cm^{-1} for the [EMIM] cation (aromatic C-H stretching) from (b). (d) The peak shift at 740 cm^{-1} for the [TFSI] anion (CF_3 stretching) from (b).

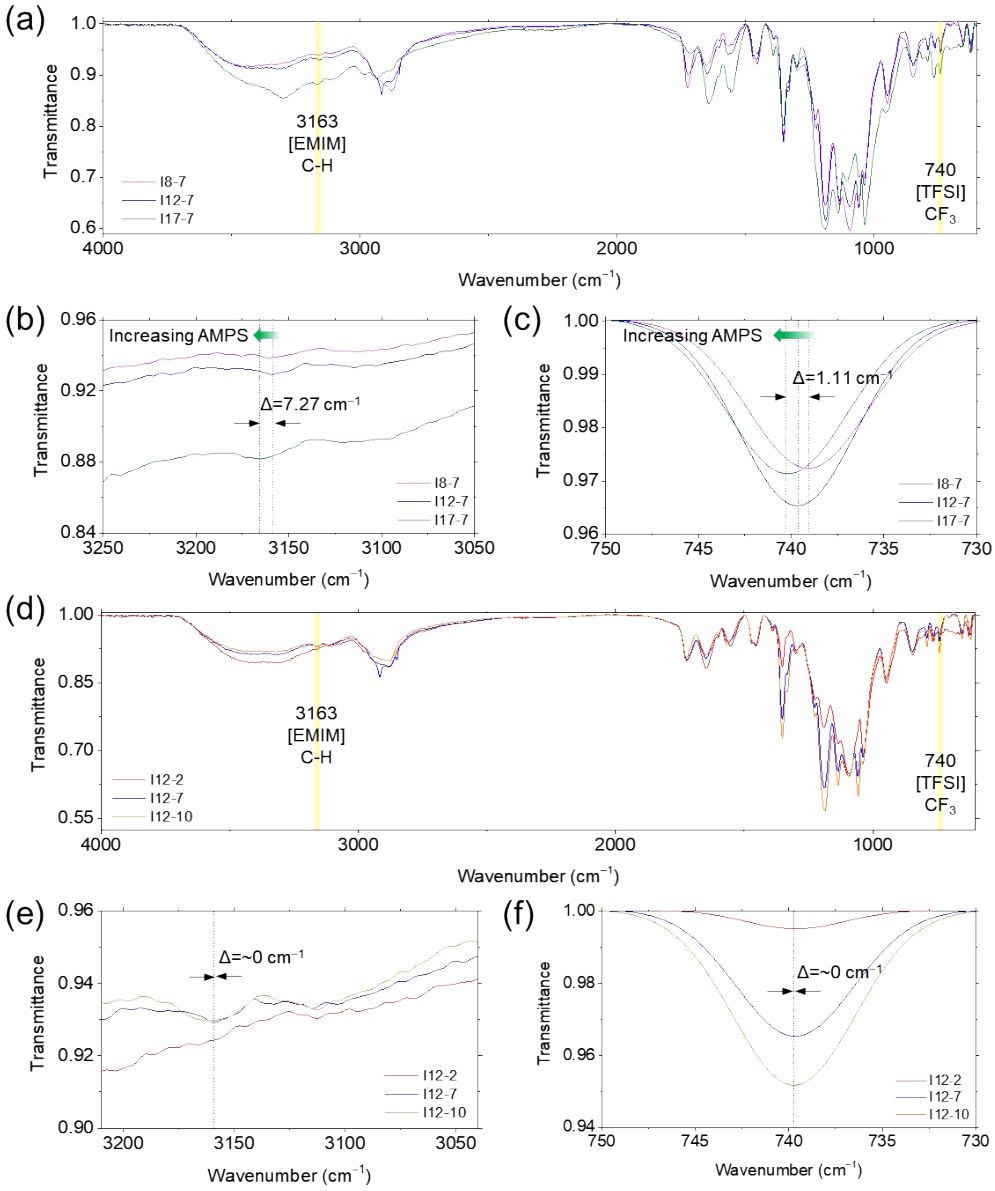

Fig. S20 | FTIR spectroscopy. (a) FTIR spectra measured for ionogel films with varying AMPS content. (b) The peak shift at 3163 cm^{-1} for the [EMIM] cation (aromatic C-H stretching) from (a). (c) The peak shift at 740 cm^{-1} for the [TFSI] anion (CF_3 stretching) from (a). (d) FTIR spectra for ionogel films with varying [EMIM][TFSI] content. (e) The peak shift at 3163 cm^{-1} for the [EMIM] cation (aromatic C-H stretching) from (d). (f) The peak shift at 740 cm^{-1} for the [TFSI] anion (CF_3 stretching) from (d).

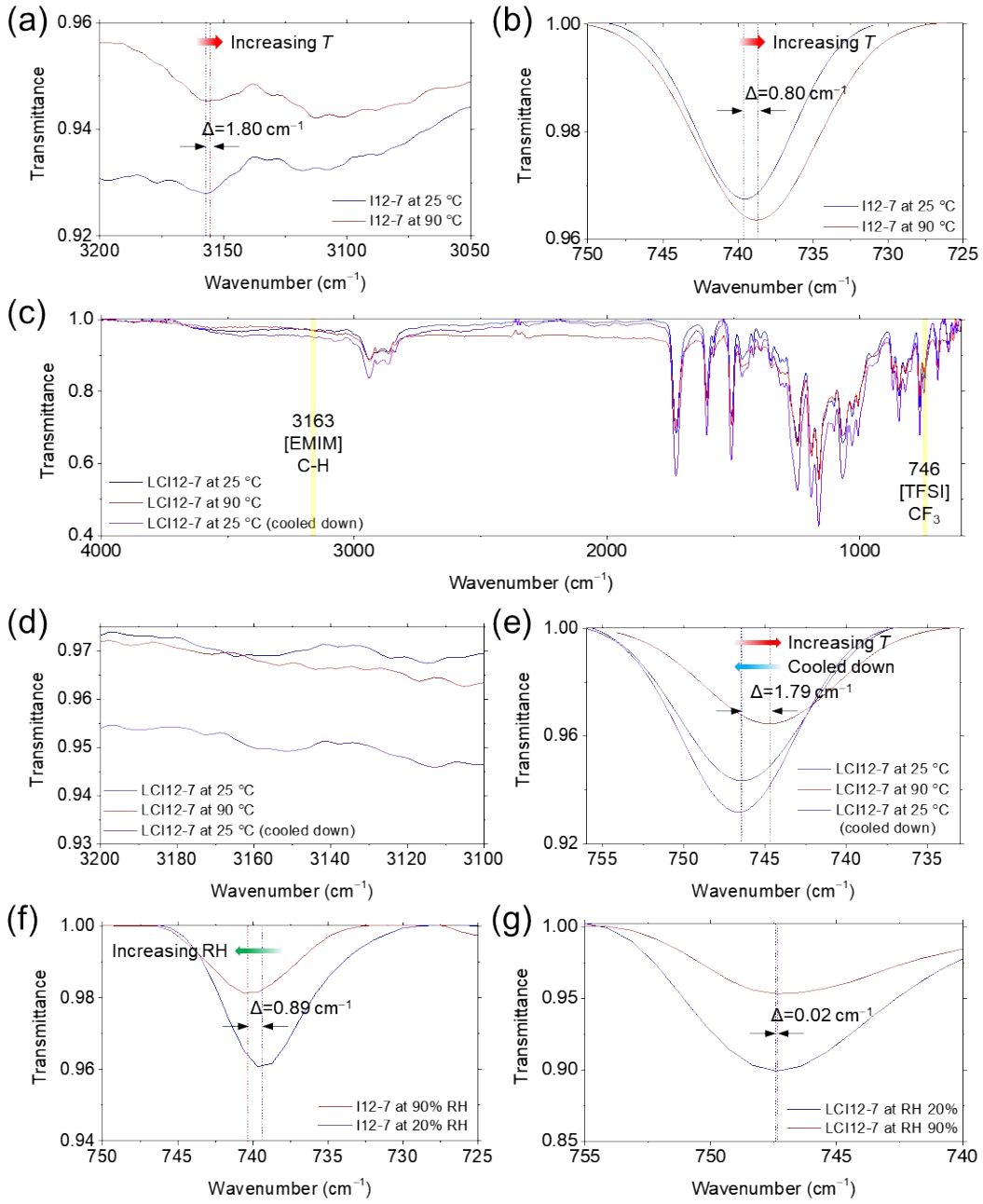

Fig. S21 | FTIR spectroscopy. (a) FTIR spectra measured for the I12-7 film at different temperatures, and the peak shift at 3163 cm^{-1} for the [EMIM] cation (aromatic C-H stretching) and (b) the peak shift at 740 cm^{-1} for the [TFSI] anion (CF_3 stretching). (c) FTIR spectra measured for the LCI12-7 films at different temperatures. (d) The peak shift at 3163 cm^{-1} for the [EMIM] cation (aromatic C-H stretching) from (c). (e) The peak shift at 740 cm^{-1} for the

[TFSI] anion (CF_3 stretching) from (c). The peak shift at 740 cm^{-1} for the [TFSI] anion (CF_3 stretching) of the (f) I12-7 film and (g) LCI12-7 film.

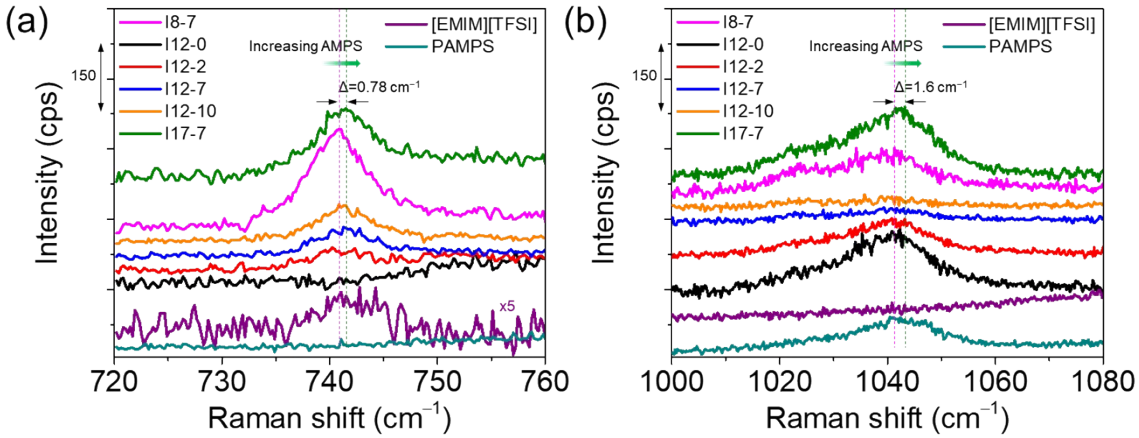

Fig. S22 | Raman spectroscopy. Raman spectra for the LCI films. (a) The Raman peak shift at 740 cm^{-1} for the [EMIM] cation (aromatic C-H stretching) and (b) the peak shift at 1040 cm^{-1} for S-O stretching of AMPS.

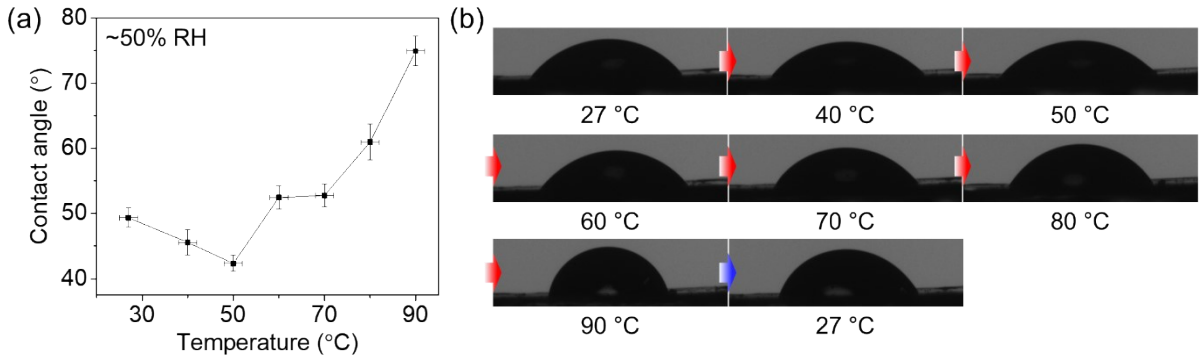

Fig. S23 | Hydrophilicity. (a) Water contact angle measurement of the LCI12-7 film at different system temperatures. (b) Photographs for the water contact angle.

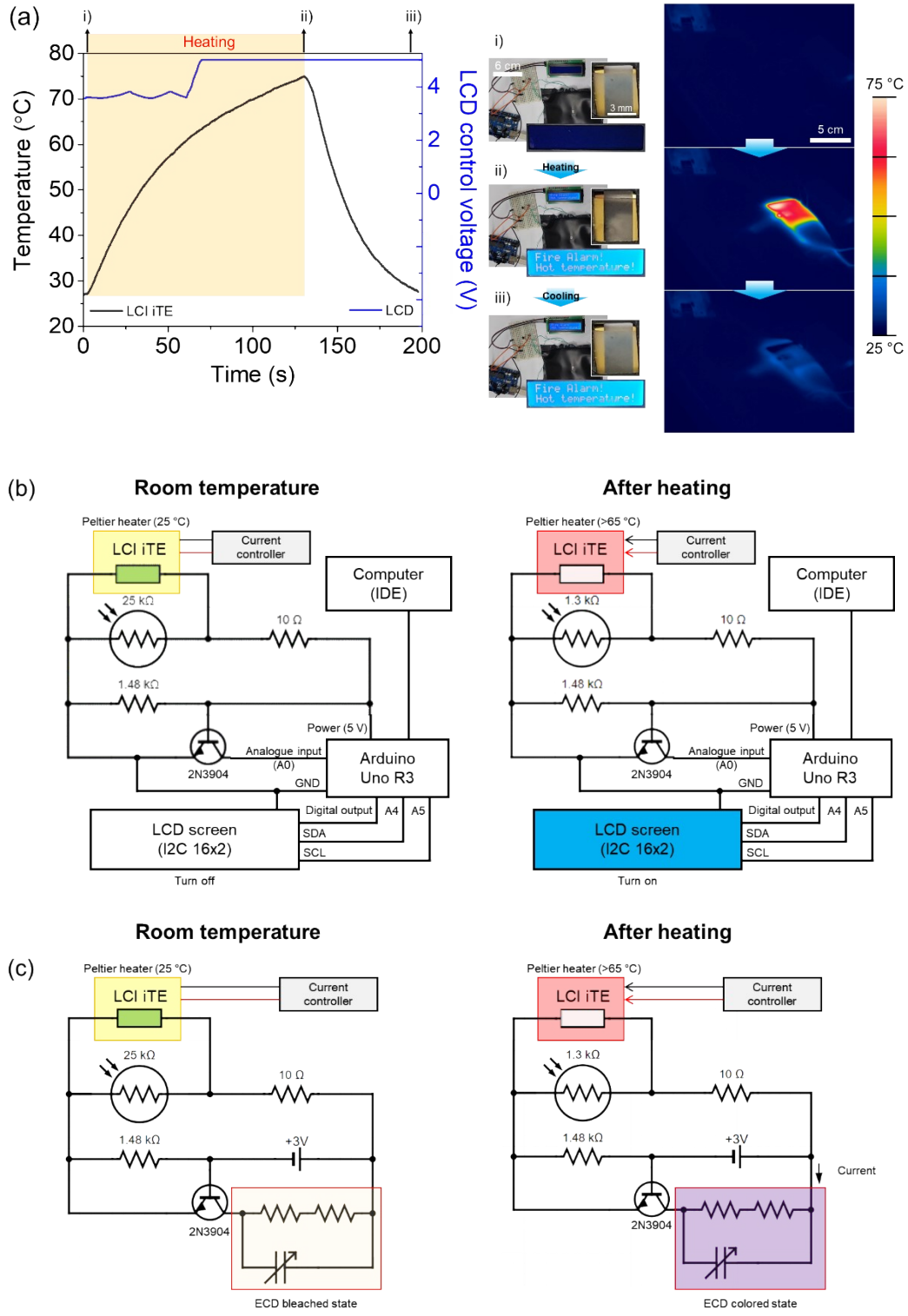

Fig. S24 | Fire alarm demonstration for intelligent electronics. (a) The system temperature and corresponding LCD control voltage operated by connecting the electronic circuit to an LCI12-7

iTE device, photoresistor, and transistor. Three thermoprogrammable states: i) Opaque device and LCD turned off. ii) Transparent device and LCD turned on after heating over 65 °C. iii) Opaque device and LCD turned on after cooling down to <65 °C. IR images show the synchronized thermal change for the system components. (b) The electrical circuit system used for operating the LCD utilizing an Arduino Uno R3 at room temperature and after heating. (c) The electrical circuit system used for operating the ECD at room temperature and after heating.

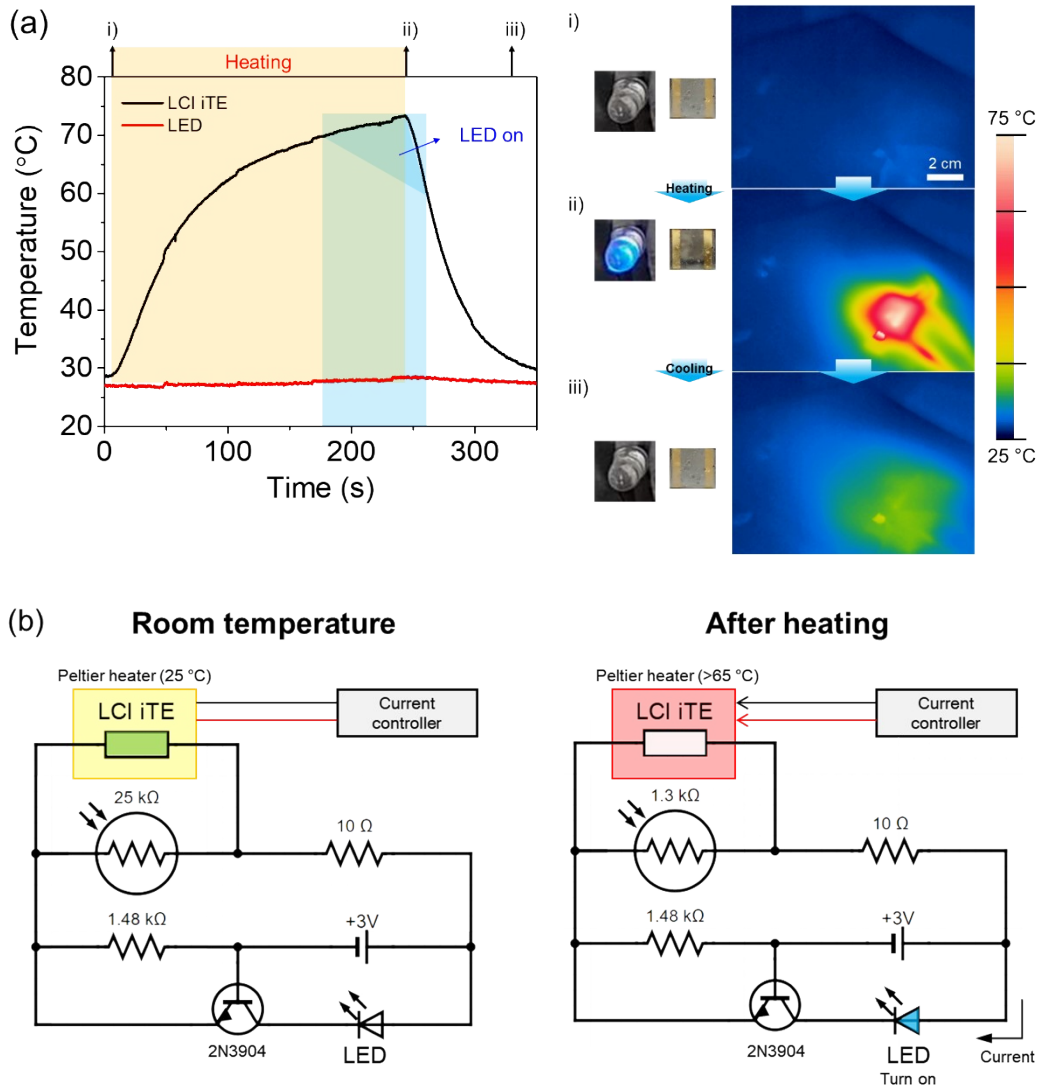

Fig. S25 | Fire alarm demonstration. (a) The system temperature and corresponding LED temperature operated by connecting to an electronic circuit comprising an LCI12-7 iTE device, photoresistor, and transistor. Three thermoprogrammable states: i) Opaque device and LED turned off. ii) Transparent device and LED turned on after heating over 65 °C. iii) Opaque device and LED turned off after cooling back to <65 °C. IR images show the synchronized thermal change for the system components. (b) Electrical circuit system used for operating the LED at room temperature and after heating.

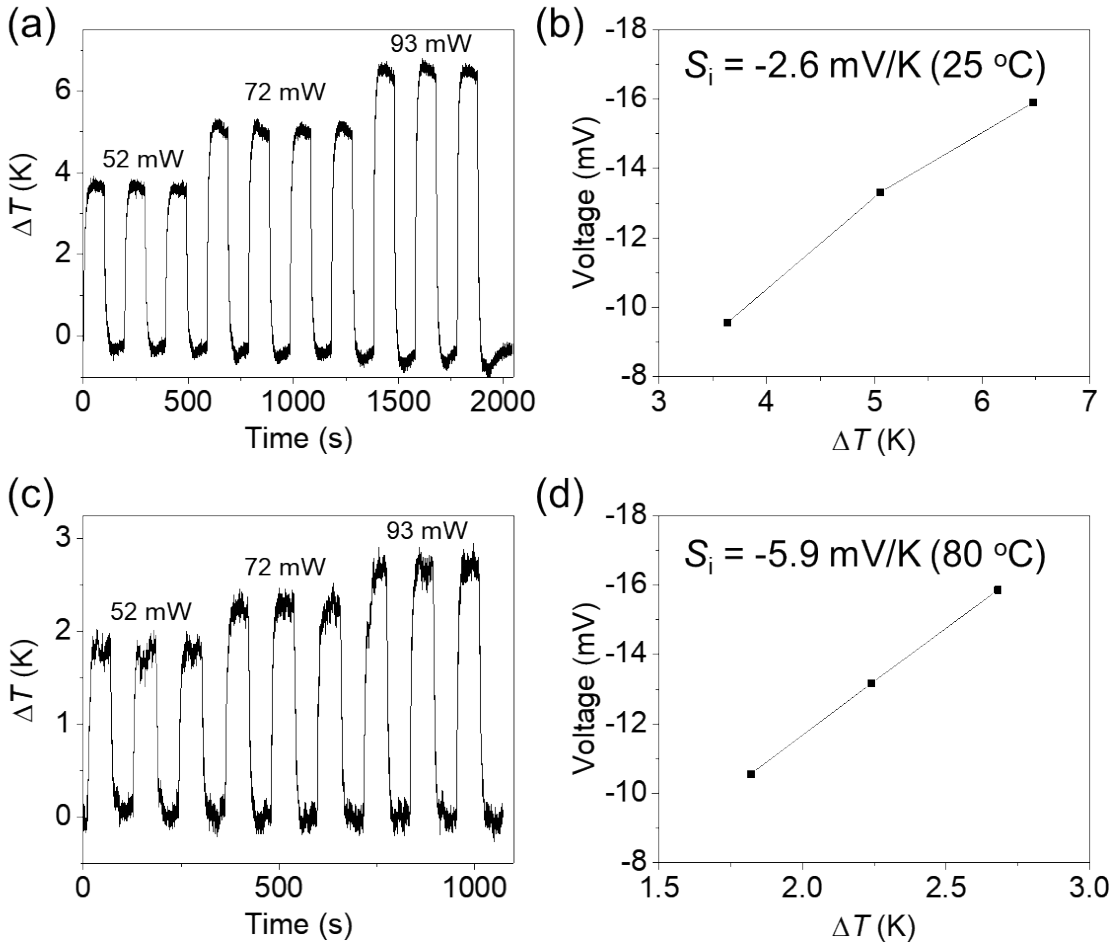

Fig. S26 | Photothermal ionic thermoelectric (PT-iTE) effect**.** (a) Temperature gradient (ΔT) obtained by the on-off application of NIR laser power used as a heat source at 25 °C. (b) Corresponding ionic Seebeck voltage obtained at different NIR laser powers at 25 °C. (c) ΔT realized by the on-off application of different NIR laser powers used as a heat source at 80 °C. (d) Corresponding ionic Seebeck voltage at different NIR laser powers at 80 °C.

Section 4. Supplementary References

1. Patterson, A. L. The Scherrer Formula for X-Ray Particle Size Determination. *Phys. Rev.* **56,** 978-982 (1939).
2. Khanum, H., Ullah, K., Murtaza, G. & Khan, S. A. Fabrication and in vitro characterization of HPMC-g-poly(AMPS) hydrogels loaded with loxoprofen sodium. *Int. J. Biol. Macromol.* **120,** 1624-1631 (2018).
3. Du, J., Zhang, L., Gao, H. & Liao, Y. Removal of methylene blue from aqueous solutions using Poly(AA-co-DVB). *J. Dispersion Sci. Technol.* **38,** 1489-1494 (2017).
4. Kiefer, J., Fries, J. & Leipertz, A. Experimental Vibrational Study of Imidazolium-Based Ionic Liquids: Raman and Infrared Spectra of 1-Ethyl-3-methylimidazolium Bis(Trifluoromethylsulfonyl)imide and 1-Ethyl-3-methylimidazolium Ethylsulfate. *Appl. Spectrosc.* **61,** 1306-1311 (2007).
5. Bulkin, B. J. The infrared spectra of complex molecules, volume 2, 2nd ed., L. J. Bellamy, Chapman and Hall, London, 1980, 299. *J. Polym. Sci. Polym. Lett. Ed.* **19,** 520-520 (1981).
6. Coates, J. Interpretation of infrared spectra, a practical approach. Citeseer; 2000.
7. Yoon, T.-H., Lee, Y.-K., Lim, B.-S. & Kim, C.-W. Degree of polymerization of resin composites by different light sources. *J. Oral. Rehabil.* **29,** 1165-1173 (2002).
8. Ferracane, J. L. & Greener, E. H. Fourier Transform Infrared Analysis of Degree of Polymerization in Unfilled Resins—Methods Comparison. *J. Dent. Res.* **63,** 1093-1095 (1984).
9. Qiao, J., Hamaya, T. & Okada, T. New highly proton-conducting membrane poly(vinylpyrrolidone)(PVP) modified poly(vinyl alcohol)/2-acrylamido-2-methyl-1-propanesulfonic acid (PVA–PAMPS) for low temperature direct methanol fuel cells (DMFCs). *Polymer* **46,** 10809-10816 (2005).
10. Gabinet, U. R. *et al.* Nanocomposites of 2D-MoS2 Exfoliated in Thermotropic Liquid Crystals. *ACS Mater. Lett.* **3,** 704-712 (2021).
11. Li, C. *et al.* Autocatalyzed interfacial thiol–isocyanate click reactions for microencapsulation of ionic liquids. *J. Mater. Sci.* **55,** 9119-9128 (2020).
12. Lee, W. J., Kwac, L. K., Kim, H. G. & Chang, J.-H. Thermotropic liquid crystalline copolyester fibers according to various heat treatment conditions. *Sci. Rep.* **11,** 11654 (2021).